ADVANCED MATERIALS TECHNOLOGIES
www.advmattechnol.de

Magnetically Activated Flexible Thermoelectric Switches Based on Interconnected Nanowire Networks

*Tristan da Câmara Santa Clara Gomes, Nicolas Marchal, Flavio Abreu Araujo, and Luc Piraux**

The use of the spin degree of freedom in thermoelectric conversion offers new functionalities for electronic devices powered by waste heat and a promising solution for sustainable technologies. Here, thermocouples formed from two dissimilar arrays of interconnected magnetic nanowires embedded in a polymer film are used to realize flexible thermoelectric switches providing optimal magnetic-field-induced control of the sign and magnitude of the thermopower. By finetuning the composition of the homogeneous and multilayered nanowires forming the thermocouple legs, an ideal on/off ratio in the switching of the thermoelectric output voltage, or a simple sign reversal can be achieved in the presence of a magnetic field. This work paves the way for flexible spin-caloritronics devices exploiting residual thermal energy for the development of thermally activated sensors and logic devices.

1. Introduction

The possibility of harnessing waste heat to power new thermal or thermoelectric devices similar to their electronic counterparts is a promising solution for achieving sustainable development goals. For example, there is a growing interest in the development of functional solid-state thermal devices,[1] such as thermal diodes,[2] thermal switches,[3] thermal transistors,[4–6] and logic devices[7,8] for improved thermal management and computing using thermal logic gates. However, one of the limiting factors of these newly developed thermal technologies is their relatively low performance characteristics.[9]

In particular, several magnetic materials and structures, such as magnetic oxides and ferromagnets, were explored for switching from a low thermal conductivity state to a high thermal conductivity state using a magnetic field trigger.[1,3,10–14] However, the contributions of phonons, electrons, and magnons to the thermal conductivity in these materials are not strongly modified by an external magnetic field. For example, the thermal conductivity of Ni nanowires[10] and Co/Cu multilayer nanostructures[11] was found to vary by a factor of 2–3 at most when a magnetic field was applied. Thus, the realization of an ideal thermal switch, characterized by almost no thermal current in the off state, remains a huge challenge. In this context, spin caloritronics, which exploits the coupling between spin and heat transport in nanostructured materials, offers new perspectives for heat-assisted spin-based logic, thermal energy conversion, and sensors applications.[15–20]

As recently suggested, the fabrication of magnetic multilayers with an appropriate composition of magnetic layers could in principle allow fine tuning of the thermoelectric current with an external magnetic field.[21–25] The spin-dependent thermoelectric effects exploit the fact that the Seebeck coefficients for spin-up and spin-down electrons are significantly different because of the large exchange splitting of d-bands.[26,27] Achieving infinitely large magneto-Seebeck effects would allow for a perfect thermoelectric switch triggered by a magnetic field. However, this imposes conditions on the spin asymmetry coefficients for the resistivity and Seebeck coefficient that are extremely difficult to fulfill in real magnetic nanosystems.[21–25]

Herein, we propose a new concept of flexible thermoelectric switch triggered by a magnetic field. Thermoelectric switching is achieved using thermocouples composed of arrays of interconnected magnetic nanowires (NWs) embedded in a 3D porous polymer film.[21,22,24,28] The two branches of the couple are formed by a multilayer structure and a homogeneous ferromagnetic material (FM), respectively.

The branch formed by permalloy (Py: $Ni_{80}Fe_{20}$)/Cu or $Co_{50}Ni_{50}$/Cu multilayers combines high room-temperature (RT) Seebeck coefficients (up to −25 μV/K) and giant magneto-Seebeck effects (up to −34%).[21,23] These giant magneto-transport phenomena are displayed in the current-perpendicular-to-plane (CPP) configuration that are easily measurable along the macroscopic in-plane dimensions of the network films.[21,22,24,29] The other branch, consisting of homogeneous NWs, has Seebeck coefficients between −30 μV K^{-1} (pure Co) and −20 μV K^{-1} (pure Ni) and shows very weak magneto-Seebeck effects.[24] Therefore, by appropriately selecting the magnetic materials and multilayers that make up the two legs of the thermocouple, we achieve high variability in the output power of the nanowire-based thermoelectric generator when the system is exposed to an external magnetic field. Interestingly, this newly developed flexible thermoelectric device is capable of switching from an "off state" ($\Delta V = 0$, with ΔV the measured output voltage from the thermocouple) to an

T. da Câmara Santa Clara Gomes, N. Marchal, F. Abreu Araujo, L. Piraux
Institute of Condensed Matter and Nanosciences
Université catholique de Louvain
Place Croix du Sud 1, Louvain-la-Neuve 1348, Belgium
E-mail: luc.piraux@uclouvain.be

The ORCID identification number(s) for the author(s) of this article can be found under https://doi.org/10.1002/admt.202101043.

DOI: 10.1002/admt.202101043

"on state" (few tens of μV, easily measurable) at the saturation field of multilayer nanowires, or vice versa at zero field. In addition, reversible switching of the thermoelectric voltage sign under an external magnetic field can also be achieved, without any degradation due to successive cycles.

2. Results and Discussion

2.1. Device Nanowire Architectures for Flexible Thermoelectrics

The flexible thermoelectric legs were fabricated by successive electrodeposition of arrays of crossed nanowires (CNWs) in a single 22 μm thick polycarbonate (PC) template from a sputtered Au cathode by adapting a previously developed method[21–23] (see **Figure 1**a and Experimental Section). Here, one branch of the thermoelectric module consists of FM/Cu multilayer CNWs while the other branch is made of magnetic CNWs of uniform composition. Next, the Au cathode is removed locally by plasma etching to create the multielectrode architecture. Thermoelectric measurements are made by placing the junction of the thermocouple in contact with the heat source while at the other extremity the two legs are thermally anchored to the heat sink (see Experimental Section). Typical dimensions of each leg are about 4 mm long and 1.5 mm wide. The legs are separated by about 2 mm. The

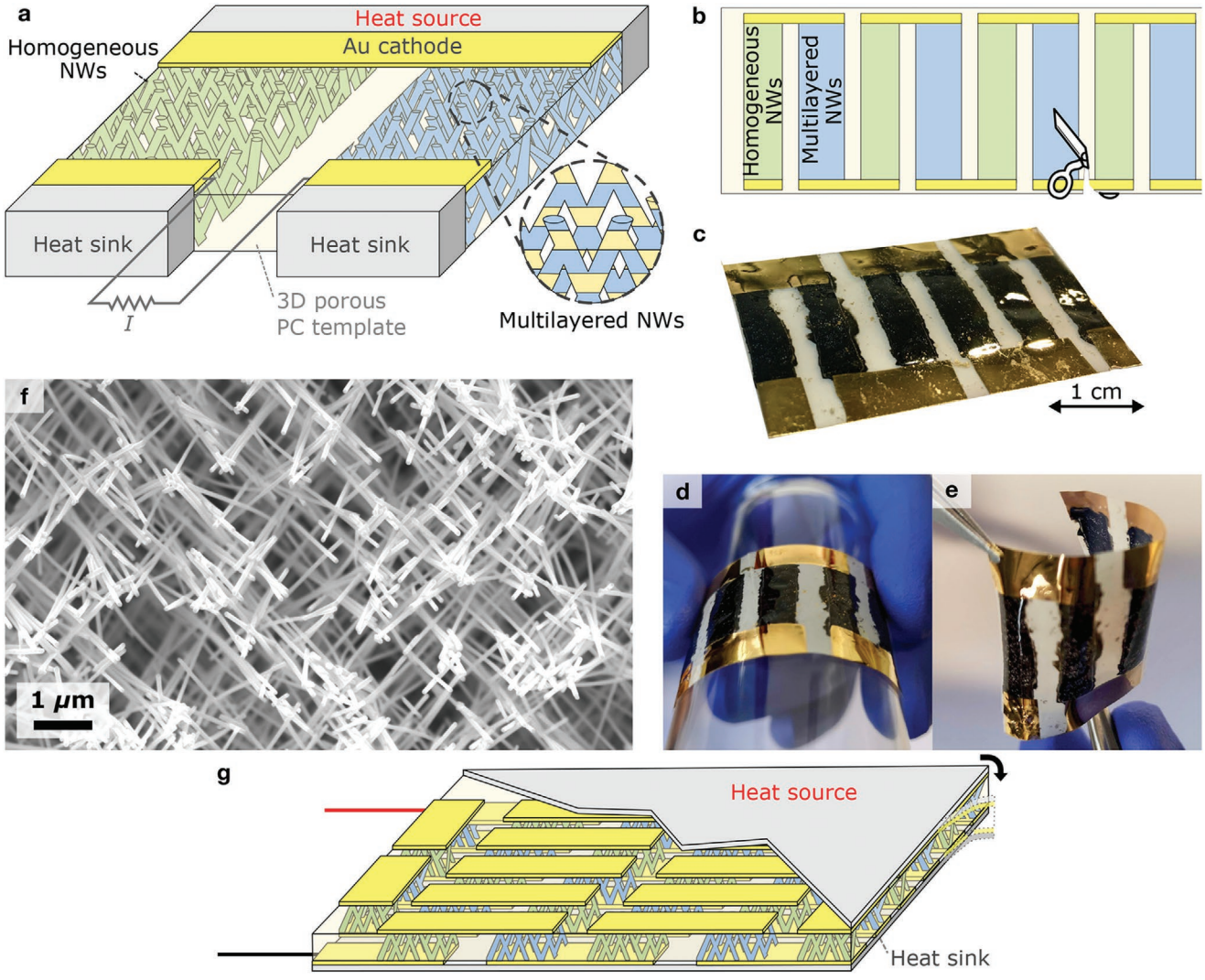

Figure 1. Flexible thermoelectric device based on interconnected nanowire networks. a) Schematic of a thermoelectric device consisting of crossed magnetic nanowires obtained by direct electrodeposition within a 3D porous polycarbonate membrane. The two thermoelectric legs are composed of homogeneous magnetic nanowires and ferromagnetic/nonmagnetic multilayer nanowires, respectively. b) Schematic of a flexible thermoelectric device consisting of several nanowire-based thermocouples, connected electrically in series and thermally in parallel. c–e) Photographs of a thermoelectric device made by connecting in series three couples of interconnected nanowire networks embedded in a porous polymer film (c) and the bendable device placed on a cylindrical support (d) or held without support (e). f) Scanning electron microscopy image of self-supported interconnected magnetic nanowires with 80 nm diameter and 3% packing density showing the 50°-tilted view of the macroscopic nanowire network film. g) Schematic of a flexible thermoelectric module consisting of pairs of interconnected homogeneous and multilayer nanowires, as in (a), with a thermal gradient perpendicular to the film surface.

size of the thermoelectric modules can however be adjusted without any real limitation. The device also takes advantage of the mechanical properties of the porous PC film allowing good flexibility and easy handling of the thermoelectric films.

Furthermore, this fabrication method allows for flexible thermoelectric films containing multiple thermocouples that can be easily cut to desired dimensions (Figure 1b). In these planar thermoelectric devices, the thermoelectric junctions are connected thermally in parallel and electrically in series. We also fabricated thermoelectric device films (Figure 1c) with three thermocouples based on CNWs. These films are flexible, shapeable (Figure 1d,e), and can be easily manipulated without damaging the electrical properties of NW-based thermoelectric modules. The scanning electron microscopy image (see Figure 1f) obtained after complete dissolution of the PC membrane of self-supporting CNWs with 80 nm diameter and 3% packing density reveals the interconnections between the NWs. It should be noted that the same fabrication technique can also be easily adapted to fabricate flexible thermoelectric modules exploiting temperature differences that occur along the film normal (Figure 1g). This alternative configuration allows the integration of a large number of thermocouples while limiting the lateral dimensions and the recovery of waste heat from complex shaped surfaces.

In this study, interconnected $Co_{50}Ni_{50}$/Cu and Py/Cu multilayer CNWs were selected as they have previously been shown to exhibit both high RT Seebeck coefficients (up to −25 μV/K) and giant magneto-thermopower effects (up to −34%).[21,23,24] Consequently, Seebeck coefficient changes of more than 5 μV K^{-1} are expected at RT between the magnetically saturated and zero-field states[21,23] (see Section A, Supporting Information for more details). The other branch consists of either pure Ni CNWs or homogeneous Co_xNi_{1-x} alloy CNWs of controlled composition. The CoNi alloy CNWs achieve Seebeck coefficients between −30 μV K^{-1} (pure Co) and −20 μV K^{-1} (pure Ni) at RT.[24] The choice of the combination of the $Co_{50}Ni_{50}$/Cu multilayer system and the Co_xNi_{1-x} alloy was motivated by the simultaneous achievement of a maximum variation of the Seebeck coefficient with an external magnetic field, as well as a similar Seebeck coefficient for both legs of the thermocouple in the magnetically saturated or in the zero-field state. The same arguments apply to the thermocouple made of Py/Cu multilayers and the Co_xNi_{1-x} alloy (see Section B, Supporting Information for details regarding the material selection).

The measured voltage of the nanowire-based thermocouple generated by a temperature gradient ΔT turns out to be

$$\Delta V = \int_{T_0}^{T_0+\Delta T} (S_{HM}(T) - S_{ML}(T))\mathrm{d}T \quad (1)$$

where T_0 is the heat-sink base temperature and S_{HM} and S_{ML} are the Seebeck coefficients of the homogeneous CNWs and multilayer CNWs, respectively. Since the Seebeck coefficient of homogeneous CNWs shows a very small variation in magnetic field, the field dependence of the output voltage of thermocouples is mainly due to FM/Cu multilayer CNWs.[24]

2.2. Controlled Output Voltage of Thermocouples Made of Nanowire Networks

Figure 2a shows the thermoelectric voltage ΔV recorded on $Co_{50}Ni_{50}$/Cu-Co_xNi_{1-x} thermocouples at zero magnetic field and for an applied field H = 7.5 kOe as a function of the Co content x. The heat sink keeps the cold side of thermoelectric module at RT and the resistive heater was used to create a temperature difference ΔT = 10 K. The larger absolute values of ΔV at H = 0 (Figure 2a) obtained following the increase in Co content x are attributed to the corresponding increase in the negative thermopower of the homogeneous Co_xNi_{1-x} CNWs. In the saturated state (H = 7.5 kOe), the curve shifts upward by about 40 μV, which is in agreement with the magneto-thermoelectric effect of the $Co_{50}Ni_{50}$/Cu CNW networks reported previously (see Section A, Supporting Information). The thermoelectric voltages obtained at H = 0 and 7.5 kOe across the thermocouple can be fine-tuned by controlling the alloy composition of the homogeneous CNW leg, as shown in Figure 2a. While the values of ΔV are always negative regardless of the composition of the alloy at zero field, and for Co contents higher than about 3% at H = 7.5 kOe, the thermoelectric voltage at the saturation field changes sign and becomes positive for lower Co concentrations in the alloy. This is due to the reduction of the thermopower of CoNi alloys when the Co content is reduced, approaching the thermopower of pure Ni (around −20 μV/K). For a Co content of less than 3%, the thermopower of $Co_{50}Ni_{50}$/Cu multilayers becomes more negative than that of Co_xNi_{1-x} alloys, leading to an overall positive Seebeck coefficient for the thermocouple, as predicted by Equation (1). The $Co_{50}Ni_{50}$/Cu-Ni thermocouple also presents an interesting characteristic as the thermoelectric voltages obtained at zero field and at saturation field show the same magnitude voltage, but of opposite signs (Figure 2a). A qualitatively similar behavior is obtained for thermocouples composed of Py/Cu multilayer CNWs and homogeneous Co_xNi_{1-x} CNWs (Figure 2b). As the negative Seebeck coefficients of Py/Cu CNWs (S = −19.7 and −24.8 μV K^{-1} at zero applied field and saturation field, respectively) are significantly higher than those of $Co_{50}Ni_{50}$/Cu CNWs (S = −16.2 and −21.7 μV K^{-1} at zero applied field and saturation field, respectively),[24] the ΔV values reported in Figure 2b are shifted upward compared to those reported in Figure 2a.

Figure 2c,d compare the temperature evolution of the thermoelectric voltages (for ΔT = 10 K) of the $Co_{50}Ni_{50}$/Cu-Co_xNi_{1-x} and Py/Cu-Co_xNi_{1-x} thermocouples, respectively. As the first type of thermocouple is composed of magnetic alloys of a similar nature, the ΔV values obtained at zero field and at saturation field show, as expected, a relatively small variation over the whole considered temperature range, whatever the Co content of the Co_xNi_{1-x} alloy (Figure 2c). On the contrary, the temperature dependencies at H = 0 and H = 7.5 kOe are more pronounced for the Py/Cu-Co_xNi_{1-x} thermocouples (Figure 2d), due to the strong temperature variations in both the Seebeck coefficient and the magneto-Seebeck effect previously observed in Py/Cu CNWs[23,24] (see Sections A and B, Supporting Information). In addition, the deviation between the output values obtained at zero field and those obtained at saturation field increases with decreasing temperature, which

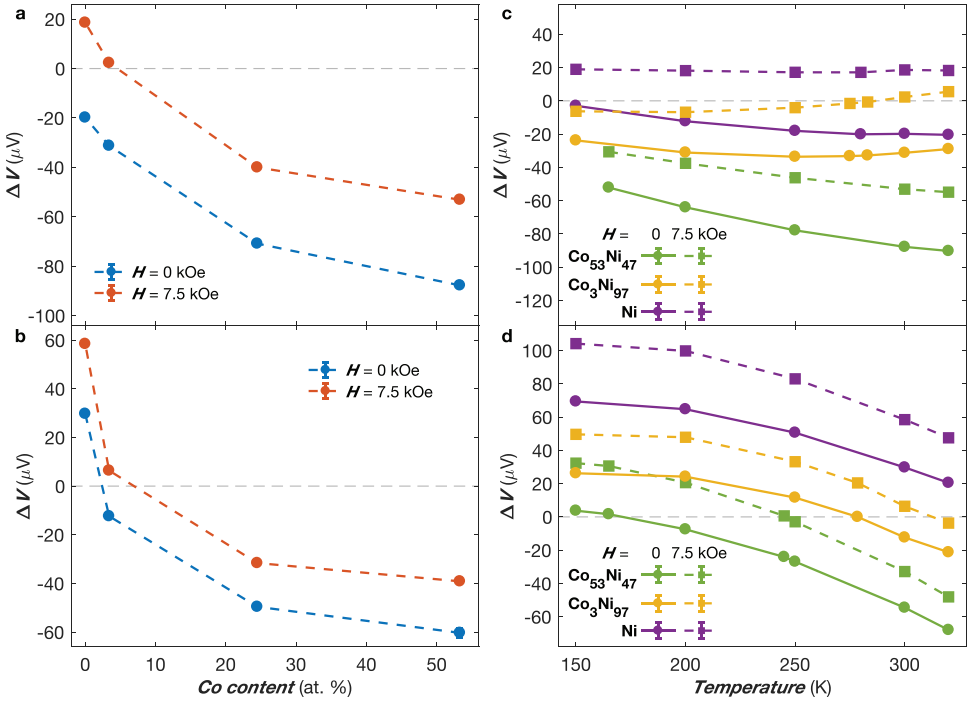

Figure 2. Device characterization as a function of composition and temperature. a,b) Variation of the thermoelectric voltage ΔV obtained at $H = 0$ and $H = 7.5$ kOe as a function of the Co content x in thermocouples formed by $Co_{50}Ni_{50}$/Cu-Co_xNi_{1-x} (a) and Py/Cu-Co_xNi_{1-x} (b) crossed nanowires. The heat sink keeps the cold side of thermoelectric module at room temperature and $\Delta T = 10$ K. c,d) Temperature dependence of the thermoelectric voltage ΔV obtained at $H = 0$ and $H = 7.5$ kOe for $\Delta T = 10$ K in thermocouples formed by interconnected nanowire networks made of $Co_{50}Ni_{50}$/Cu and Co_xNi_{1-x} with $x = 0\%$, 3%, and 53% (c) and of Py/Cu and Co_xNi_{1-x} with $x = 0\%$, 3%, and 53% (d). The error bars are smaller than the markers, reflecting the uncertainty of the voltage and temperature measurements and is set to two times the standard deviation, gathering 95% of the data variation (see Section D, Supporting Information for details).

also reflects the strong enhancement of the magneto-Seebeck effect of Py/Cu CNWs at low temperature.[23,24] Overall, the deviations between the ΔV values at zero field and saturation field are smaller for Py/Cu-Co_xNi_{1-x} thermocouples than for $Co_{50}Ni_{50}$/Cu-Co_xNi_{1-x} thermocouples, but the more pronounced temperature dependence of the former system allows for better control of the thermocouple output. In contrast, the $Co_{50}Ni_{50}$/Cu-Co_xNi_{1-x} thermocouples have increased temperature stability.

2.3. Magnetically Activated Thermoelectric Switches

A thermoelectric switch where the output power of the thermocouple is cancelled when the external magnetic field saturates the magnetization of the multilayer is depicted in **Figure 3**a. Such a device operating at RT can be obtained from a thermocouple comprising two CNW networks made of Co_3Ni_{97} alloy and $Co_{50}Ni_{50}$/Cu multilayers. From the variation of the electrical resistance of the thermocouple in an external in-plane magnetic field (red curve in Figure 3b), it appears that the magnetoresistance (MR) signal is mainly due to the giant magnetoresistance effect induced by the multilayer structure. Indeed, the MR ratio defined as $MR = (R_0 - R_{sat})/R_0$, where R_0 and R_{sat} are the resistances at $H = 0$ and $H = 7.5$ kOe, respectively, reaches about 28% at RT. This value is only slightly lower than those previously recorded on $Co_{50}Ni_{50}$/Cu CNWs[21] (see Section C, Supporting Information for further information).

In addition, the magnetic field variation of the thermoelectric voltage ΔV (blue curve in Figure 3b, for $\Delta T = 10$ K) is very similar to that of the MR signal, indicating that $\Delta V(H)$ is dominated by the magneto-Seebeck effect depending on the multilayer structure[21,24] (see Section A, Supporting Information for further information). As found in previous works,[21–25,30] the large amplitude of the magneto-thermopower signal is assigned to the large spin-dependent Seebeck coefficients of 3d ferromagnets.[26,27] The thermoelectric voltage varies from $\Delta V_0 \approx -33$ μV at $H = 0$ to $\Delta V_{sat} \approx 0$ at $H = 7.5$ kOe. The voltage levels exhibited by the junction are easy measured and the use of such devices in a TTL or CMOS logic circuit is technically feasible. Several degrees of freedom can be combined, such as assembling junctions in series, increasing temperature gradient and/or amplifying the resulting signal to the required logic voltage levels. All these optimizations would drastically reduce the need for a high amplification.

The time traces of temperature and thermoelectric voltage ΔV (Figure 3c,d) illustrate the behavior of a thermoelectric switch (for successive ΔT values of 1, 4, and 10 K) which leads to the cancellation of the thermocouple output power in the presence of an external magnetic field. The heater is switched on after 100 s, resulting in an increase in temperature at the thermocouple junction. After 700 s, a magnetic field of $H = 7.5$ kOe is applied, leading to a vanishing output voltage.

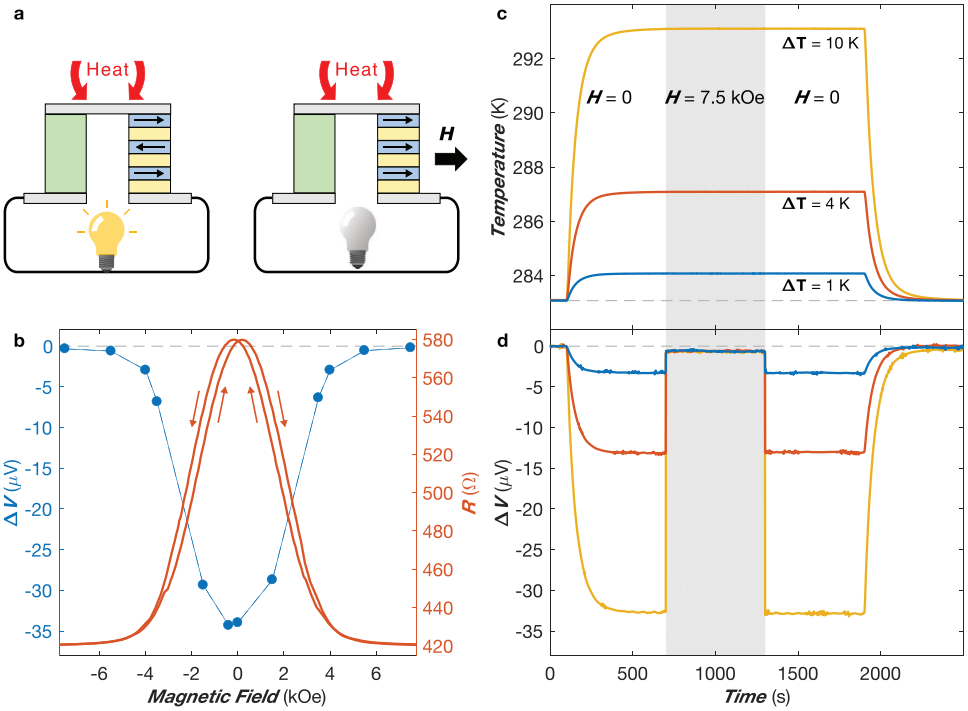

Figure 3. Switching with magnetic field—the "off" state at saturation field. a) Schematic of a thermoelectric switch between the "on" state (at zero field) and the "off" state (at saturation field). b) Magnetic field dependence of the thermoelectric voltage ΔV for a temperature difference $\Delta T = 10$ K and of the electrical resistance R of a thermocouple composed of a leg of Co_3Ni_{97} crossed nanowires and a leg of $Co_{50}Ni_{50}$/Cu crossed nanowires at room temperature. c,d) Time dependence of the hot side temperature (c) and thermoelectric voltage ΔV (d) for a thermocouple made of Co_3Ni_{97} and $Co_{50}Ni_{50}$/Cu crossed nanowires. The heater is switched on after 100 s. The grey area indicates the presence of an external magnetic field of 7.5 kOe. Error bars in (b) are smaller than the markers, reflecting the uncertainty of the voltage and temperature measurements and set to two times the standard deviation, gathering 95% of the data variation (see Section D, Supporting Information for details).

The fully realized transition from an on state and an off state of a thermoelectric switch occurs over a very short time interval, which is only limited by the field rise time. However, the magnetic field slope speed may be optimized using a more localized magnetic field generator. Finally, the magnetic field and the heating are successively switched off in the time sequence shown in Figure 3c,d.

Alternatively, we also have fabricated a thermoelectric switch for which an output signal requires the application of an external magnetic field (**Figure 4**a). This particular device was obtained using a thermocouple consisting of two legs made of Py/Cu and Co_3Ni_{97} CNWs. The thermoelectric voltage and electrical resistance of the thermocouple display very similar field dependencies (Figure 4b). The MR ratio is close to 10% at RT which is ≈40% lower than that previously recorded on Py/Cu interconnected CNWs[23] (see Section C, Supporting Information for further information). The output voltage of the thermocouple is close to zero at $H = 0$ and reaches about +21 μV in the saturated state (Figure 4b). Following the same time sequence of heating/magnetic field activation and deactivation as defined in Figure 3c,d, the time traces of temperature and thermoelectric voltage ΔV (Figure 4c,d) determined for successive runs (with $\Delta T = 1$, 4, and 10 K) illustrate the behavior of a thermoelectric switch that gives no output voltage at zero field and requires the application of an external magnetic field to generate thermoelectric power. Although this is a second order effect, small peaks appear in the thermocouple voltage when the hot source is turned off. This can be interpreted by different thermal relaxation dynamics of the two thermoelectric legs.

Interestingly, such NW-based thermocouples can be used for achieving control of the thermoelectric voltage polarity (**Figure 5**a). In this case, magnetic saturation of the multilayer system leads to a change in sign of the thermoelectric voltage. Such a device can be obtained in particular by choosing $Co_{50}Ni_{50}$/Cu and Ni CNWs as thermoelements of the thermocouple. For this thermocouple, the MR ratio at RT reaches about 28%. The field evolution of ΔV (Figure 5b) shows that the thermoelectric voltage can be controlled in a range between −20 μV (at zero field) and +18 μV (at $H = 7.5$ kOe) for a temperature difference of $\Delta T = 10$ K. Furthermore, the thermoelectric voltage can be switched between three distinct states (−1, 0, and +1) achieved at $H = 0$, 3, and 7.5 kOe, respectively. The tunability of the magnitude and sign of the thermoelectric voltage supplied by the $Co_{50}Ni_{50}$/Cu-Ni CNWs thermocouple is clearly seen in the thermoelectric voltage time traces (Figure 5c,d) obtained for $\Delta T = 1$, 4, and 10 K.

It should be noted that other combinations of materials can be used to obtain magnetic thermoelectric switches triggered by a magnetic field with the same functionality as illustrated in Figures 3–5. In addition, the material composition of the thermoelectric legs can be adjusted to allow the device to operate at the desired temperature, using the data reported in Figure 2c,d. Furthermore, our devices are robust, that is,

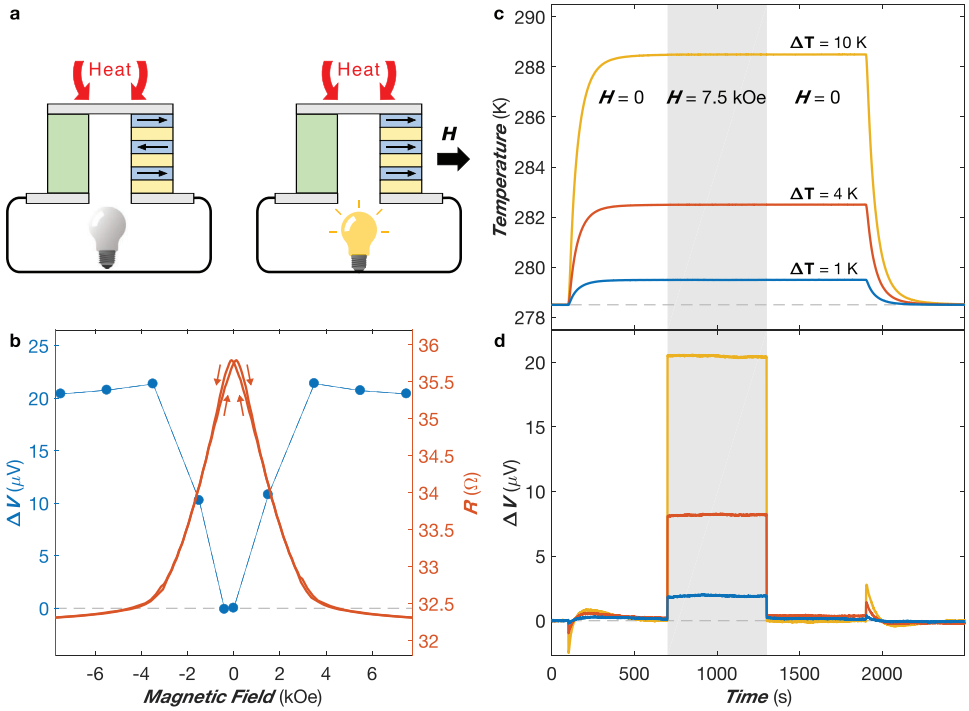

Figure 4. Switching with magnetic field—the "off" state at zero field. a) Schematic of a thermoelectric switch between the "off" state (at zero field) and the "on" state (at saturation field). b) Magnetic field dependence of the thermoelectric voltage ΔV for a temperature difference $\Delta T = 10$ K and of the electrical resistance R of a thermocouple composed of a leg of Co_3Ni_{97} crossed nanowires and a leg of Py/Cu crossed nanowires at room temperature. c,d) Time dependence of the hot side temperature (c) and thermoelectric voltage ΔV (d) for a thermocouple made of Co_3Ni_{97} and Py/Cu crossed nanowires. The heater is switched on after 100 s. The grey area indicates the presence of an external magnetic field of 7.5 kOe. Error bars in (b) are smaller than the markers, reflecting the uncertainty of the voltage and temperature measurements and set to two times the standard deviation, gathering 95% of the data variation (see Section D, Supporting Information for details).

capable of switching their thermoelectric output voltage on demand without any limitation on the number of cycles associated with the magnetic field change and without cycles-induced deviation of the thermoelectric outputs at zero and saturation field.

3. Conclusion

In this article, we propose 3D arrays of interconnected magnetic nanowires embedded in a polymer film as a unique platform for designing flexible thermoelectric devices with added functionalities. The fabrication technique is fast, cheap, versatile and reliable, with no limitations on device size. These results demonstrate a new concept of thermoelectric magnetic switch, obtained from a thermocouple film whose legs are formed of homogeneous Co_xNi_{1-x} nanowire arrays and multilayer nanowire arrays ($Co_{50}Ni_{50}$/Cu or Py/Cu), the latter showing giant magneto-Seebeck effects. By adjusting the composition of the magnetic thermoelectric legs, a switching of the thermoelectric voltage between zero and a few tens of μV can be achieved when the external magnetic field is turned on or off, without any degradation due to successive cycles. Furthermore, the $Co_{50}Ni_{50}$/Cu-Ni crossed nanowire thermocouple exhibits a controlled sign change of the thermoelectric voltage depending on whether it is subjected to an external magnetic field or not. Such reversible switching of the thermoelectric voltage sign has only recently been demonstrated in fragile gold atomic wire junctions by varying the mechanical stress applied to the junction.[31]

From a practical point of view, the magnetic control of the magnitude and sign of the thermopower, opens the route toward to the development of thermally activated sensors and logic devices exploiting the residual thermal energy from hot surfaces with complex geometries, or even from the human body. In addition, Onsager reciprocity between Peltier and Seebeck effects implies that a switchable Seebeck voltage results in a switchable Peltier heat flow. In a recent work, Adams et al.[32] showed that a Peltier module can be seen as an active thermal switch that opens and closes under an activation current. Furthermore, we have recently demonstrated that multilayer nanowire arrays can magnetically control the Peltier thermal flux.[21,22] Therefore, the flexible thermoelectric modules developed here can be used as thermal switches, offering future prospects for precise thermal management. Besides, as ferromagnets have recently been shown to be particularly suitable for active cooling applications,[33] interconnected metal nanowire networks offer good application prospects in this field. On this basis, the present work also contributes to the emergence of flexible thermoelectric materials and devices to address the rapid development of miniature, lightweight, and functional portable electronic devices.[34]

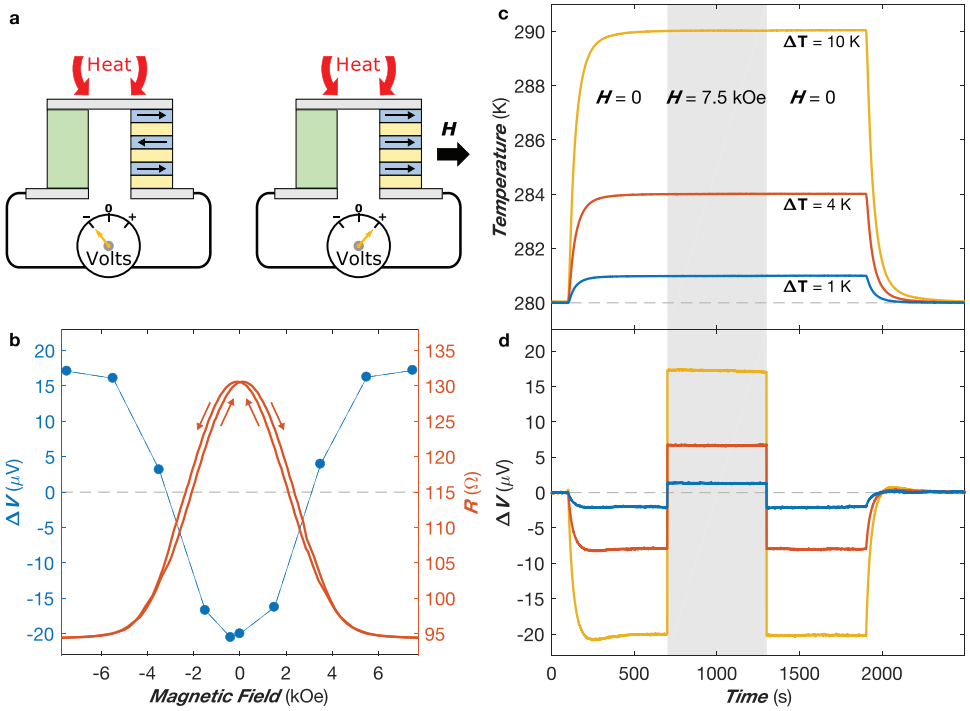

Figure 5. Magnetic field induced polarity reversal of thermoelectric voltage. a) Schematic of the thermoelectric voltage generation device with polarity reversal induced by an external magnetic field. b) Magnetic field dependence of the thermoelectric voltage ΔV for a temperature difference $\Delta T = 10$ K and of the electrical resistance R of a thermocouple composed of a leg of Ni crossed nanowires and a leg of $Co_{50}Ni_{50}$/Cu crossed nanowires at room temperature. c,d) Time dependence of the hot side temperature (c) and thermoelectric voltage ΔV (d) for a thermocouple made of Ni and $Co_{50}Ni_{50}$/Cu crossed nanowires. The heater is switched on after 100 s. The grey area indicates the presence of an external magnetic field of 7.5 kOe. Error bars in (b) are smaller than the markers, reflecting the uncertainty of the voltage and temperature measurements and set to two times the standard deviation, gathering 95% of the data variation (see Section D, Supporting Information for details).

4. Experimental Section

Device Fabrication: The fabrication technique of 3D CNW networks[21–23] was adapted to fabricate thermoelectric junction made of two CNW legs embedded into a single flexible polymer film. The NW-based thermocouples were fabricated by two successive direct electrodeposition into a single 22 µm thick track-etched PC template with crossed nanochannel networks. The PC films were exposed to heavy ions (Ar^{9+}) along four direction making an angle of about 20–25° with respect to the PC film normal and along four in-plane directions making 90° with each other. The tracks generated were then revealed using a NaOH aqueous solution at 70 °C during a controlled time to obtain a 3D network of cylindrical nanopores with well defined diameters of 80 nm. The template porosity (void fraction) was about 3%.

Then, a Cr/Au bilayer was sputtered on one side of the template to serve as cathode during the electrochemical deposition. The adhesive layer of Cr was set to 3 nm and the Au layer was set to 700 nm which ensured a complete coverage of the pores. A rectangular rubber mask was used to deposit the CNWs at selected locations within the porous membrane. The thermoelectric junctions were fabricated by depositing two nearby parallel rectangular CNW networks, as schematically depicted in Figure 1a, one CNW network consisting of homogeneous Co_xNi_{1-x} CNWs with controlled alloying composition, the other consisting of FM/Cu multilayer CNWs (FM = $Co_{50}Ni_{50}$ or Py).

Co_xNi_{1-x} CNWs were deposited by direct electrodeposition at constant potential of −1 V from home-made electrolyte solutions containing the Ni^{2+} and Co^{2+} cations, as described elsewhere.[29,35,36] The alloying composition was controlled by modifying the Co^{2+} cation concentration from 5 to 170 mM within the electrolyte solutions containing 1 M of Ni^{2+}, which allowed for a Co content x from ≈3% up to ≈53%. For such alloy compositions, it has been shown from XRD measurements that Co_xNi_{1-x} CNWs exhibited an FCC structure.[35] For Py/Cu multilayer nanowires, a FCC phase was also found.[37] Pure Ni CNWs were deposited from electrolyte solution containing 1 M of Ni at a potential of −1.1 V. For the FM/Cu multilayered structure, FM and Cu layers were stacked along the CNW axis using a pulsed electrodeposition technique from single home-made electrolyte containing the FM and Cu^{2+} cations. The $Co_{50}Ni_{50}$/Cu or Py/Cu CNWs were deposited following the procedure described elsewhere[21] and,[23] respectively. All deposition were made in the potentiostatic mode at RT. Then, the Cr/Au cathode was locally removed by a plasma etching process to create a multi-electrode design, as reported elsewhere.[21,22]

Device Measurement: The electrical resistance of each thermocouple circuit was measured by injecting a DC current through the thermoelectric CNW legs and measuring the voltage drop. A magnetic field up to ±7.5 kOe, enough to saturate the multilayer CNW system, was applied in the plane of the CNW network device. For the magnetoresistance measurements, the field was swept from +7.5 to −7.5 kOe, back and forth.

For measuring the thermoelectric modules, a resistive heat source was used to induce a heat current through the two thermoelectric CNW legs and create a temperature differential ΔT, while the heat sinks were maintained at the desired temperature T_0, as illustrated in Figure 1a. This created a temperature differential ΔT at the edges of the two CNW network legs. The temperature at the junction electrode and of the heat sinks were recorded by Cernox sensors. The current in the resistive heater was set to induce ΔT of 1, 4, and 10 K between the heat source and heat sinks. Meanwhile, the hot junction generated a voltage difference ΔV across the CNW legs. The external magnetic field was either directly applied at +7.5 kOe in the plane of the CNW network to saturate the multilayer CNW system, or it was swept from +7.5 to −7.5 kOe. All thermoelectric measurements were performed under vacuum.

Supporting Information

Supporting Information is available from the Wiley Online Library or from the author.

Acknowledgements

N.M. acknowledges the Research Science Foundation of Belgium (FRS-FNRS) for financial support (FRIA grant). F.A.A. is a postdoctoral researcher of the FNRS. The authors would like to thank Dr. E. Ferain and the it4ip Company for supplying polycarbonate membranes.

Conflict of Interest

The authors declare no conflict of interest.

Data Availability Statement

The data that support the findings of this study are available from the corresponding author upon reasonable request.

Keywords

3D nanowire networks, flexible thermoelectrics, spin caloritronics, thermoelectric switch

Received: August 26, 2021
Published online:

[1] T. Swoboda, K. Klinar, A. S. Yalamarthy, A. Kitanovski, M. Muñoz Rojo, *Adv. Electron. Mater.* **2021**, *7*, 2170008.
[2] C. Dames, *J. Heat Transfer* **2009**, *131*, 061301.
[3] G. Wehmeyer, T. Yabuki, C. Monachon, J. Wu, C. Dames, *Appl. Phys. Rev.* **2017**, *4*, 041304.
[4] B. Li, L. Wang, G. Casati, *Appl. Phys. Rev.* **2006**, *88*, 143501.
[5] W. C. Lo, L. Wang, B. Li, *J. Phys. Soc. Jpn.* **2008**, *77*, 054402.
[6] A. Sood, F. Xiong, S. Chen, H. Wang, D. Selli, J. Zhang, C. J. McClellan, J. Sun, D. Donadio, Y. Cui, E. Pop, K. E. Goodson, *Nat. Commun.* **2018**, *9*, 4510.
[7] L. Wang, B. Li, *Phys. Rev. Lett.* **2007**, *99*, 177208.
[8] F. Paolucci, G. Marchegiani, E. Strambini, F. Giazotto, *Phys. Rev. Appl.* **2018**, *10*, 024003.
[9] K. Klinar, T. Swoboda, M. Muñoz Rojo, A. Kitanovski, *Adv. Electron. Mater.* **2021**, *7*, 2000623.
[10] H.-T. Huang, M.-F. Lai, Y.-F. Hou, Z.-H. Wei, *Nano Lett.* **2015**, *15*, 2773.
[11] J. Kimling, R. B. Wilson, K. Rott, J. Kimling, G. Reiss, D. G. Cahill, *Phys. Rev. B* **2015**, *91*, 144405.
[12] J. Cho, M. D. Losego, H. G. Zhang, H. Kim, J. Zuo, I. Petrov, D. G. Cahill, P. V. Braun, *Nat. Commun.* **2014**, *5*, 4035.
[13] J. Shin, M. Kang, T. Tsai, C. Leal, P. V. Braun, D. G. Cahill, *ACS Macro Lett.* **2016**, *5*, 955.
[14] X. Zhao, J. C. Wu, Z. Y. Zhao, Z. Z. He, J. D. Song, J. Y. Zhao, X. G. Liu, X. F. Sun, X. G. Li, *Appl. Phys. Rev.* **2016**, *108*, 242405.
[15] G. E. W. Bauer, E. Saitoh, B. J. van Wees, *Nat. Mater.* **2012**, *11*, 391.
[16] S. R. Boona, R. C. Myers, J. P. Heremans, *Energy Environ. Sci.* **2014**, *7*, 885.
[17] M. Zeng, Y. Feng, G. Liang, *Nano Lett.* **2011**, *11*, 1369.
[18] J. Ren, J.-X. Zhu, *Phys. Rev. B* **2013**, *88*, 094427.
[19] X.-J. Gao, P. Zhao, G. Chen, *Org. Electron.* **2018**, *62*, 277.
[20] P. Zhao, *J. Magn. Magn. Mater.* **2019**, *489*, 165381.
[21] T. da Câmara Santa Clara Gomes, F. Abreu Araujo, L. Piraux, *Sci. Adv.* **2019**, *5*, eaav2782.
[22] F. Abreu Araujo, T. da Câmara Santa Clara Gomes, L. Piraux, *Adv. Electron. Mater.* **2019**, *5*, 1800819.
[23] N. Marchal, T. da Câmara Santa Clara Gomes, F. Abreu Araujo, L. Piraux, *Nanoscale Res. Lett.* **2020**, *15*, 137.
[24] T. da Câmara Santa Clara Gomes, N. Marchal, F. Abreu Araujo, L. Piraux, *Nanomaterials* **2020**, *10*, 11.
[25] N. Marchal, T. da Câmara Santa Clara Gomes, F. Abreu Araujo, L. Piraux, *Nanomaterials* **2021**, *11*, 5.
[26] T. Farrell, D. Greig, *J. Phys. C: Solid State Phys.* **1970**, *3*, 138.
[27] M. C. Cadeville, J. Roussel, *J. Phys. F: Metal Physi.* **1971**, *1*, 686.
[28] L. Piraux, T. da Câmara Santa Clara Gomes, F. Abreu Araujo, J. De La Torre Medina, in *Magnetic Nano- and Microwires*, 2nd ed. (Ed: M. Vázquez), Elsevier, New York **2020**, pp. 801–831.
[29] T. da Câmara Santa Clara Gomes, N. Marchal, F. Abreu Araujo, Y. Velázquez Galván, J. de la Torre Medina, L. Piraux, *Nanomaterials* **2021**, *11*, 221.
[30] J. Shi, S. S. P. Parkin, L. Xing, M. B. Salamon, *J. Magn. Magn. Mater.* **1993**, *125*, L251.
[31] A. Aiba, F. Demir, S. Kaneko, S. Fujii, T. Nishino, K. Tsukagoshi, A. Saffarzadeh, G. Kirczenow, M. Kiguchi, *Sci. Rep.* **2017**, *7*, 7949.
[32] M. J. Adams, M. Verosky, M. Zebarjadi, J. P. Heremans, *Int. J. Heat Mass Transfer* **2019**, *134*, 114.
[33] M. Adams, M. Verosky, M. Zebarjadi, J. Heremans, *Phys. Rev. Appl.* **2019**, *11*, 054008.
[34] Z. Fan, Y. Zhang, L. Pan, J. Ouyang, Q. Zhang, *Renewable Sustainable Energy Rev.* **2021**, *137*, 110448.
[35] T. da Câmara Santa Clara Gomes, J. De La Torre Medina, M. Lemaitre, L. Piraux, *Nanoscale Res. Lett.* **2016**, *11*, 466.
[36] Y. G. Velázquez Galván, T. da Câmara Santa Clara Gomes, L. Piraux, J. De La Torre Medina, *J. Magn. Magn. Mater.* **2020**, 166615.
[37] J. L. Maurice, D. Imhoff, P. Etienne, O. Durand, S. Dubois, L. Piraux, J. M. George, P. Galtier, A. Fert, *J. Magn. Magn. Mater.* **1998**, *184*, 1.

